THE JOURNAL OF BIOLOGICAL CHEMISTRY VOL. 284, NO. 17, pp. 11498–11506, April 24, 2009

Interactions of Lipopolysaccharide and Polymyxin Studied by NMR Spectroscopy*[S]

Received for publication, August 25, 2008, and in revised form, January 27, 2009 Published, JBC Papers in Press, February 25, 2009, DOI 10.1074/jbc.M806587200

Jiri Mares[‡], Sowmini Kumaran[‡], Marina Gobbo[§], and Oliver Zerbe[‡1]

From the [‡]Institute of Organic Chemistry, University of Zurich, Winterthurerstrasse 190, Zurich CH 8057, Switzerland and the [§]Department of Chemical Sciences, University of Padova, via Marzolo 1, Padova I-35131, Italy

In the light of occurrence of bacterial strains with multiple resistances against most antibiotics, antimicrobial peptides that interact with the outer layer of Gram-negative bacteria, such as polymyxin (PMX), have recently received increased attention. Here we present a study of the interactions of PMX-B, -E, and -M with lipopolysaccharide (LPS) from a deep rough mutant strain of *Escherichia coli*. A method for efficient purification of biosynthetically produced LPS using reversed-phase high-performance liquid chromatography in combination with ternary solvent mixtures was developed. LPS was incorporated into a membrane model, dodecylphosphocholine micelles, and its interaction with polymyxins was studied by heteronuclear NMR spectroscopy. Data from chemical shift mapping using isotope-labeled LPS or labeled polymyxin, as well as from isotope-filtered nuclear Overhauser effect spectroscopy experiments, reveal the mode of interaction of LPS with polymyxins. Using molecular dynamics calculations the complex of LPS with PMX-B in the presence of dodecylphosphocholine micelles was modeled using restraints derived from chemical shift mapping data and intermolecular nuclear Overhauser effects. In the modeled complex the macrocycle of PMX is centered around the phosphate group at GlcN-B, and additional contacts from polar side chains are formed to GlcN-A and Kdo-C, whereas hydrophobic side chains penetrate the acyl-chain region.

Cellular membranes segregate the interior of cells from their surroundings and therefore are crucial to maintain cells as autonomously functioning systems (1). The chemical constituents of outer membranes from mammalian cells and bacteria are fundamentally different (2). The mammalian outer membranes are largely formed by phospholipid bilayers, whereas additional coating structures are present covering these in bacteria. In Gram-positive bacteria a thick peptidoglycan layer is built around the phospholipid bilayer. In Gram-negative bacteria, the peptidoglycan structure is much thinner and coated by an additional phospholipid-containing bilayer, whose outer leaflet is mainly composed of lipopolysaccharides (LPSs)[2] (3). LPS are high molecular weight, strongly negatively charged molecules, which for smooth LPS can be divided in three regions: the lipid A portion of LPS inserts into the phospholipidic membrane and in many Gram-negative bacteria consists of a di-glucosamine diphosphate with 5 to 7 fatty acid chains extending to one side of the disaccharide. The lipid A is appended to a region (the inner core) of 8–12 variable sugars (including the negatively charged 3-deoxy-D-manno-oct-2-ulosonate (Kdo) units) and 3–8 phosphate residues. To the inner core is covalently associated the *O*-antigen, an oligosaccharide chain of variable length and chemical composition, depending on the exact type of LPS.

Sepsis caused by Gram-negative bacteria is a serious source of mortality in many clinical cases, accounting for ~200,000 deaths in the U.S. annually (see David (4) and references therein). The primary trigger for sepsis was identified as LPS, and LPS-neutralizing agents are therefore valuable therapeutics. Antimicrobial peptides against Gram-negative bacteria can interfere with the integrity of this LPS layer. PMX-B is considered as the "gold standard" for LPS-sequestering agents. Polymyxin-B, -M, and -E are characterized by a heptapeptide ring and a fatty acid tail (see Fig. 1). These highly cationic decapeptides contain six diaminobutyric acid (Dab) residues, a macrocylic ring involving residues 4–10, and an acyl chain coupled to the N terminus. Severe toxic side effects have limited their usage to treatments against bacteria resistant against most other antibiotics such as *Pseudomonas aeruginosa*. The interaction of LPS with various antimicrobial peptides has been the subject of a number of studies (4–15). In some of these, the conformation of the LPS-bound peptides was established using transferred NOE effects, and the complex between LPS and the peptides was established by docking the transferred NOE-derived peptide conformer to LPS (11), whose coordinates were taken from the crystal-structure of FhuA-bound LPS (16).

The emphasis of this work was to obtain experimental data on the LPS·PMX complex, thereby allowing a detailed understanding of the interacting moieties. Because LPS in the outer membrane of *Escherichia coli* cells is integrated into a phospholipid bilayer, it was studied while integrated into phospholipid micelles to better mimic the natural environment. In our studies we used LPS from the deep rough mutant D31m4 of *E. coli* (Re-LPS). Biosynthetic production of the latter and its isolation

* This work was supported by the Swiss National Science Foundation (Grant 3100A0-11173).

[S] The on-line version of this article (available at http://www.jbc.org) contains supplemental Tables S1, S2, and S10–S13, Figs. S3–S9, and text.

[1] To whom correspondence should be addressed. Tel.: 41-44-635-4263; Fax: 41-44-635-6882; E-mail: oliver.zerbe@oci.uzh.ch.

[2] The abbreviations used are: LPS, lipopolysaccharide; Kdo, 3-deoxy-D-manno-oct-2-ulosonate; PMX, polymyxin; Dab, diaminobutyric acid; NOE, nuclear Overhauser effect; Re-LPS, LPS from the deep rough mutant D31m4 of *E. coli*; HPLC, high-performance liquid chromatography; DPC, dodecylphosphocholine; MALDI-TOF, matrix-assisted laser desorption ionization time-of-flight; MES, 4-morpholineethanesulfonic acid; MD, molecular dynamics; TOCSY, total correlation spectroscopy; HM, hydroxymyristoyl; LM, lauroxymyristoyl.

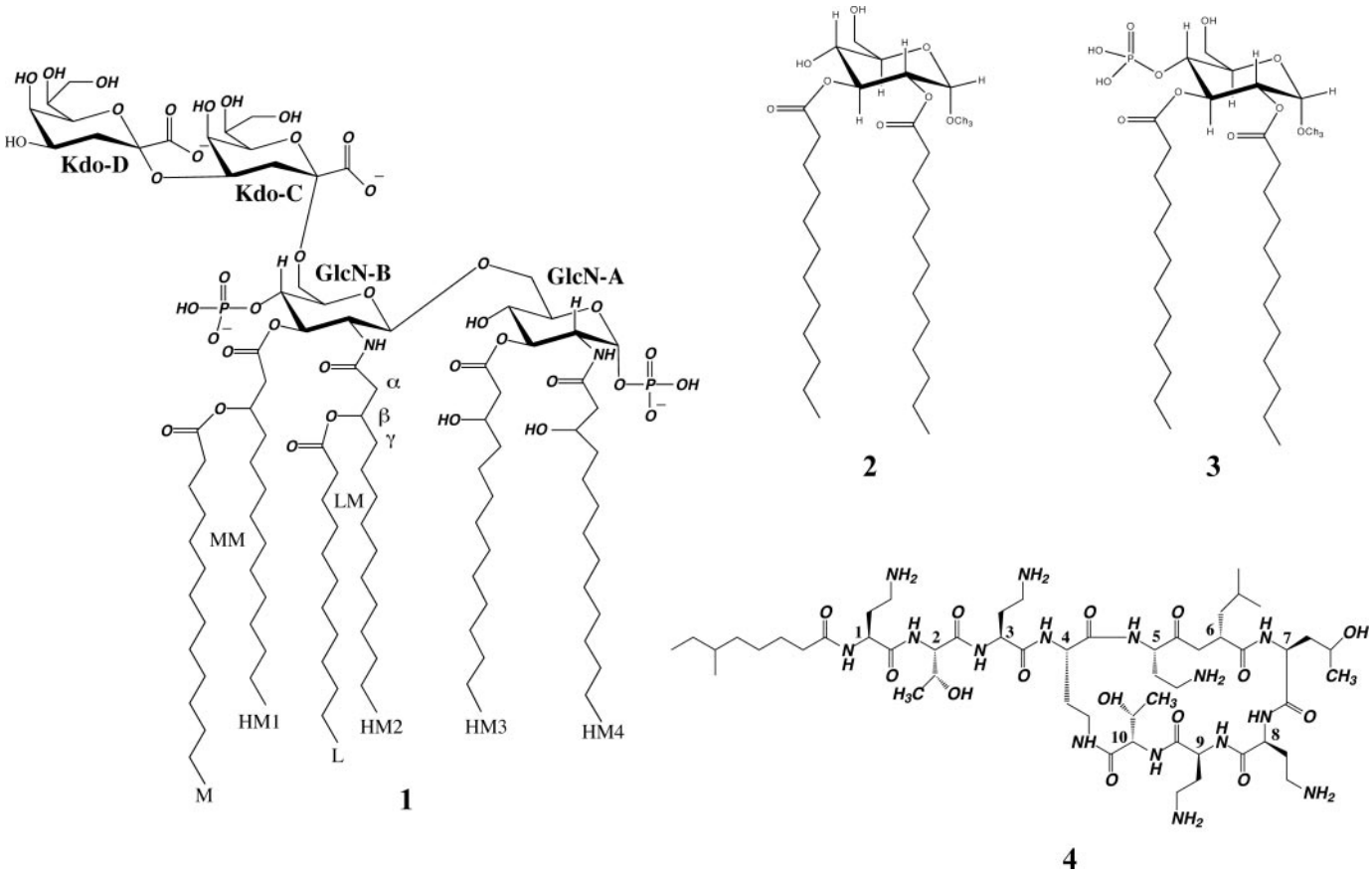

FIGURE 1. **Chemical structures of LPS from the D31m4 *E. coli* strain (*1*), the two model compounds for LPS (*2* and *3*), and PMX-M (*4*).** Note that in PMX-B residue D-Leu-6 is replaced by D-Phe and Thr-7 is replaced by Leu, and in polymyxin-E Thr-7 is replaced by Leu. In the text, the glycosidic residues of LPS are identified with the letters *A–D*, starting from the far right GlcN residue.

and purification from the membrane fraction of the corresponding cells was described in literature. However, to facilitate purification by reversed-phase HPLC, the phosphate groups were methylated (17). The modified LPS was investigated in detail by NMR (18). Because interactions with the charged phosphate groups were proposed to be important for binding antimicrobial peptides, we developed an HPLC-based method that allows purification of LPS in its natural (non-methylated) form (Fig. 1). ^{13}C,^{15}N-Labeled LPS from the deep rough mutant strain was isolated and purified to chemical homogeneity. Extensive use of heteronuclear solution NMR techniques allowed characterization of LPS embedded in DPC micelles and facilitated the study of its interactions with polymyxins from different organisms. The interaction studies relied on chemical shift mapping techniques and isotope-filtered NOEs and allowed direct probing for the interaction sites.

EXPERIMENTAL PROCEDURES

Materials—$^{15}NH_4Cl$ was purchased from Spectra Isotopes (Columbia, MD), perdeuterated DPC-d38 (99%-d), and D_2O were ordered from Cambridge Isotope Laboratories (Andover, MA). Methyl-5-doxylstearic acid was bought from Aldrich (Buchs, Switzerland). The Re-LPS-producing strain D31m4 was purchased from the *E. coli* Genetic Resource Center, New Haven, CT. The PMX-M-producing strain *Paenibacillus kobensis* M was obtained from Prof. J. C. Vederas, and PMX-B and -E were purchased from Sigma-Aldrich.

Production of ^{13}C-Labeled LPS from the E. coli Strain D31m4—Cells from the D31m4 strain of *E. coli* were grown at 37 °C to an optical density of ~1.0 at 600 nm on minimal medium M9 using 4 g of [^{13}C]glucose and 1 g of ^{15}N ammonium chloride supplemented with 100 mg of Trp, His, and Pro per liter.

After harvest cells were resuspended in 50 ml of ice-cold water and pelleted down. To the pellet a minimum amount of cold water was added such that a thick paste was formed. LPS together with other components was precipitated through addition of 90 ml of ice-cold methanol and centrifuged at 8000 × *g*. The pellet was resuspended in 90 ml of ice-cold acetone, homogenized, and centrifuged again, followed by another acetone washing step. The lyophilized cells (~0.7 g) were taken up in 50 ml of a phenol:chloroform: petroleum ether (4:10:16, v/v) solvent mixture and centrifuged at 9,200 × *g*, after which most of the LPS was contained in the supernatant. The remaining pellet was extracted once more to increase the yield in LPS. The supernatant was concentrated under a nitrogen stream, and 2 ml of water was added dropwise to the concentrate. A waxy precipitate was formed followed by three cycles of washing with methanol and subsequent centrifugation. Thereafter the pellet was dried and lyophilized, after which it could only be resuspended in water using repetitive additions of small amounts of water followed by sonication. Solubilization was improved

upon adding aqueous 0.1 M EDTA in the first portions. The resulting solution was centrifuged at 200,000 × *g* overnight and then lyophilized.

Chromatography used the following solvents: solvent A (methanol:chloroform:water, 57:12:31, v/v) and solvent B (methanol:chloroform, 29.8:70.2, v/v). The lyophilized pellet after resuspension in the mixture of solvent A and aqueous EDTA was directly loaded onto the HPLC column. For optimal purification of LPS a gradient system involving ternary solvent mixtures was used consisting of solvent A in 10 mM NH_4Cl and solvent B in 50 mM NH_4Cl. LPS (6 mg) was dispersed in a two phase system formed from 0.8 ml of solvent A and 0.2 ml of 0.1 M aqueous EDTA (pH 7) and loaded directly onto the RP-C8 column. Chromatographic separation was achieved using the following gradient of solvents A and B: 2 column volumes of 2% B, 3 column volumes (2–17% B), 3.5 column volumes (17–27% B). UV detection was impossible, and hence fractions were lyophilized and their content checked by MALDI-TOF using 6-aza-2-thiothymine as the matrix. Elution of the desired LPS occurred around 20–23% of solvent B.

Production of $^{13}C,^{15}N$-Labeled PMX-M from P. kobensis M—The producer strain, *P. kobensis* M, was grown aerobically at 30 °C on tryptic soy agar. A 1-liter batch of M9 medium was inoculated with a 10-ml *P. kobensis* M preculture (1% inoculum). After a total growth time of 16–24 h at 30 °C with shaking (200 rpm), the cells were removed by centrifugation (1 h, 10,000 rpm), and the supernatant was then passed through a Amberlite XAD-16 column. After washing with 30% ethanol, active peptide was then eluted with 70% isopropanol, which was adjusted to pH 2 (pH meter reading) with 12 N HCl.

All fractions were assessed for antimicrobial activity using a well plate assay. The contents of the active fraction were applied to a Superdex peptide 10/300 column (Amersham Biosciences). Fractions were collected for 3 column volumes with pure Milli-Q Water and each assayed for activity. All active fractions were pooled, concentrated, and applied as 20% isopropanol solutions to C_{18} reversed-phase HPLC. Complete purification required two separate steps of C_{18} HPLC. The first separation used a gradient of water/isopropanol (0.1% trifluoroacetic acid), from 20% to 50% isopropanol, and the second step a water/methanol gradient (0.1% trifluoroacetic acid), from 45% to 85% methanol. PMX-M eluted at around 55%. Finally, 8–10 mg of pure PMX-M was obtained as slightly yellowish powder from a 1-liter culture, and its chemical nature was verified by electrospray ionization-mass spectrometry (experimental mass: 1224.73 Da; theoretical mass: 1223.57 Da).

During all steps of expression and purification, antimicrobial activity was monitored by inhibition of growth of an indicator strain. Agar plates were prepared by inoculating molten tryptic soy agar (40 g/liter) with a culture of the indicator organism *E. coli* (1.0% inoculum). Small wells (~4.6-mm diameter) were made in the seeded agar plates, and 50 μl of filtered culture supernatant was added to the wells. Plates were incubated at 30 °C, and the growth of the indicator organism was visible after ~3 h (19).

NMR Spectroscopy—LPS samples used for assignment purposes contained ~1 mM LPS, 300 mM d_{38}-DPC in 40 mM d_{13}-MES D_2O buffer, pD = 5.8. Resonance positions required very small changes to adapt to $^{13}C,^{1}H$ HSQC spectra in 40 mM acetate buffer at pH 4.4. All interaction studies were performed in 40 mM acetate buffer, 300 mM d_{38}-DPC in D_2O, or H_2O/D_2O 9/1 (pH 4.4). Measurements of interactions between LPS and PMX by chemical shift mapping observing LPS resonances utilized a 350 μM solution of $^{15}N,^{13}C$ Re-LPS and equimolar unlabeled peptides. Chemical shift changes in PMX-M were monitored on a 200 μM solution of $^{15}N,^{13}C$-labeled PMX-M and equimolar unlabeled Re-LPS. No further salt was present in the measurements except for initial attempts to optimize conditions for $^{15}N,^{1}H$ HSQC spectra in the PMX-M·Re-LPS sample (see below). To satisfy requirements for better sensitivity higher concentrations of doubly labeled LPS (500 μM) were used in the isotope-filtered NOESY experiments (200-ms mixing time). Due to the moderate dissociation constant the experiment in fact monitored transferred NOEs; therefore, 3-fold excess of unlabeled PMX-E or PMX-B (2 mM solutions) were used with conditions of pH, detergent, and temperature otherwise identical to those of the shift mapping studies.

Spectra were recorded on Bruker AV-600 or AV-700 NMR spectrometer at $T = 310$ K. Proton and carbon chemical shifts were calibrated to 2,2-dimethyl-2-silapentane-5-sulfonic acid, and nitrogen shifts were referenced indirectly to liquid NH_3 (20). The spectra were processed using the Bruker Topspin 2.0 software and transferred into CARA (21) or SPARKY (22) programs for further analysis.

For chemical shift assignments of $^{13}C,^{15}N$-labeled LPS two-dimensional versions of three-dimensional double- and triple-resonance experiments were recorded. In general, experiments used coherence selection schemes via pulsed-field gradients (23) and sensitivity-enhancement building blocks (24, 25) whenever possible. For assignments of the carbon spin systems in the lipid chains and the sugar units (H)CCH experiments recorded with 4- and 12-ms DIPSI-2 C-C mixing cycles were used. Linkage of the lipid chains onto the glucosamine parts of lipid A was achieved via correlations with the amide nitrogens using HNCA and HN(CO)CA experiments. To distinguish the two Kdo units, key NOEs derived from a ^{13}C-resolved NOESY were exploited. Assignment of all resonances of polymyxin was done using HN(CO)CACB (26), HNCACB (27), and (H)CCH experiments (28, 29) analogous to the procedure used for proteins. Because of the small size of the peptide two-dimensional versions were recorded with a total of <12-h measuring time for acquiring all spectra. Assignments of polymyxin-B and -E were based on assignments from PMX-M adjusted by using additional two-dimensional heteronuclear spectra.

In the spin-label experiments, a 0.5 mM solution of LPS was separated into two aliquots, and to one of these 5-doxylstearate methyl ester was added so that the final concentration corresponded to approximately one spin-label per micelle. Signal intensities from the two corresponding constant-time $^{13}C,^{1}H$ HSQC were extracted, and the ratio of signal intensities from the samples with and without spin label was calculated.

Molecular Dynamics Calculations—All calculations were performed within the program GROMACS (30). Briefly, coordinates of LPS were adapted from the pdb entry 1QFF, and coordinates of polymyxin B were built using the program Ghemical (31). Parameters and topologies of PMX-B and LPS

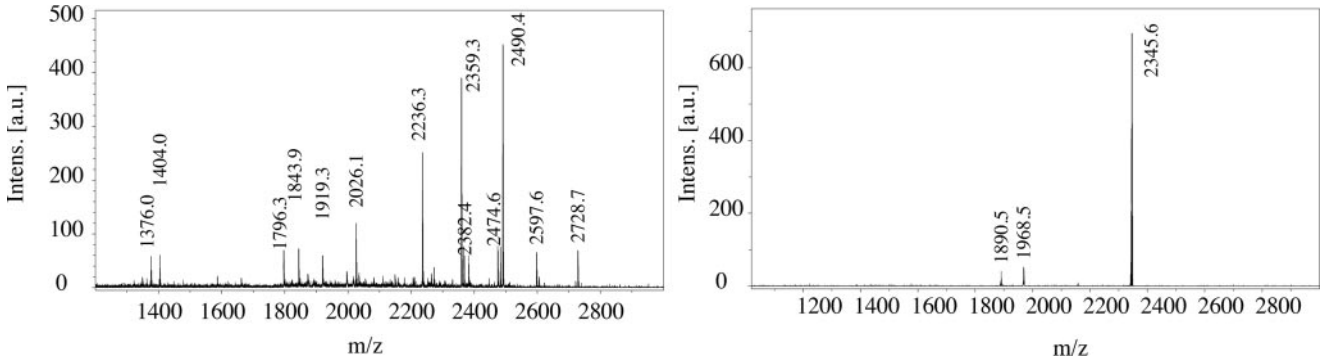

FIGURE 2. **Comparison of the MALDI-TOF mass spectrometry spectrum of commercial LPS with LPS from the deep rough D31m4 *E. coli* strain purified by the protocol that includes an additional HPLC purification step.**

as well as partial charges of PMX-B for GROMACS were established based on data from the PRODRG server (32) and the GROMOS 53a6 force field (33). Partial charges of LPS were assigned for a protonation state corresponding to experimental conditions of pH by the MPEOP method (34, 35). Parameters for DPC were derived from values for dipalmitoylphosphatidylcholine from the GROMOS force field library. A detailed description of the methodology pursued can be found in the supplemental materials. Briefly, the system was prepared as follows: (i) An initial complex between LPS and polymyxin B was prepared and equilibrated in the presence of a DPC micelle. (ii) A set of simulated annealing calculations was performed yielding 450 structures. The DPC molecules were explicitly included in the system, water molecules were substituted by implicit solvent, and the dominant NOE-derived upper distance limits were included (the force constant was set to 1000 kJ $mol^{-1}nm^{-2}$). (iii) Those structures were selected, which displayed best agreement with the chemical shift mapping data. (iv) These were then equilibrated with explicit solvent and subjected to further refinement and analysis. The latter included an assessment of the stability of the MD trajectory and a comparison of the average intermolecular distances with chemical shift mapping data.

RESULTS

Production and Purification of ^{13}C-Labeled LPS—LPS from the deep rough *E. coli* mutant D31m4 was isolated from the membrane fraction of cells grown on minimal medium containing [^{13}C]glucose and [^{15}N]H_4Cl as the sole carbon and nitrogen sources, respectively. After pentachlorphenol extraction and further purification using published protocols (3, 36) the yield was ~129 mg/liter of culture. Remaining impurities were removed by reversed-phase HPLC using a ternary solvent mixture. In this procedure the solvent system was carefully adapted to form a single phase over the whole gradient range of solvent A (methanol:chloroform:water) and solvent B (methanol:chloroform) at room temperature. Importantly, any mixture of these two solvent systems is relatively close to a two-phase system, and this condition proved to have favorable properties for dissolving LPS. MALDI-TOF spectra of LPS before and after this HPLC purification step are depicted in Fig. 2. Sufficient quantities (40 mg) of chemically pure LPS for the NMR studies could be produced from 1 liter of culture using this protocol. As demonstrated in supplemental Fig. S4 this method is capable of separating pyrophosphate from the monophosphate derivatives.

Assignment of LPS and Polymyxin Resonances—Chemical shift mapping (37) or NOE-based methods (38–40) can be used to study biomolecular interactions (see also Refs. 41–43). Both methods potentially deliver information on interacting moieties but require assignments of chemical shifts. The best chemical shift dispersion is usually available in heteronuclear shift correlation spectra (*e.g.* ^{15}N,^{1}H HSQC or ^{13}C,^{1}H HSQC spectra). Importantly, these experiments still work well in the presence of the increased line widths that are usually present in systems that are stably anchored into phospholipids micelles. In addition, as was unfortunately the case in some of our applications, additional exchange broadening occurred upon complex formation. To probe integration of LPS into DPC micelles and to study its interaction with peptides, we decided to label it with ^{13}C and ^{15}N isotopes and use the corresponding HSQC spectra for chemical shift mapping.

To assign all signals in the constant-time ^{13}C,^{1}H HSQC spectrum (44), three-dimensional (H)CCH-TOCSY spectra (28, 29) served for assignment of spin systems (Fig. 3). The C,H-plane of the HNCA (45, 46) and HN(CO)CA (45) experiments was used to establish scalar connectivities between terminal carbons of the fatty acid chains and C-2 of the glucosamine moieties. Unsubstituted hydroxymyristoyl (HM) can be distinguished from lauroxymyristoyl (LM) and thereby helps to differentiate between GlcN-A from GlcN-B. Due to chemical shift degeneracies, it was impossible to assign chains of the fatty acids (myristoyl of myristoxy-myristoyl and lauroyl of LM). The two Kdo units were linked and thereby distinguished from each other using several key NOEs in the three-dimensional ^{13}C-NOESY spectra. The unique chemical shift of the C3 moiety of Kdo is located in a region separated from all other sugar resonances and was used as a starting point for sequential assignment. Only the methylene group C3 of Kdo-C is expected to receive an NOE from H(C6) of GlcN-B. This assignment was additionally supported by the fact that H(C6) and H(C7) of Kdo-C displayed an NOE to H(C3) of both Kdo units, which is unlikely to be the case for H(C6) of Kdo-D. The ^{1}H,^{13}C and ^{15}N chemical shifts of LPS in DPC micelles are reported in Table 1.

Topology of LPS and Polymyxin Insertion into the DPC Micelle—To probe whether LPS properly inserts into the DPC micelles, and whether the sugar moieties really protrude into

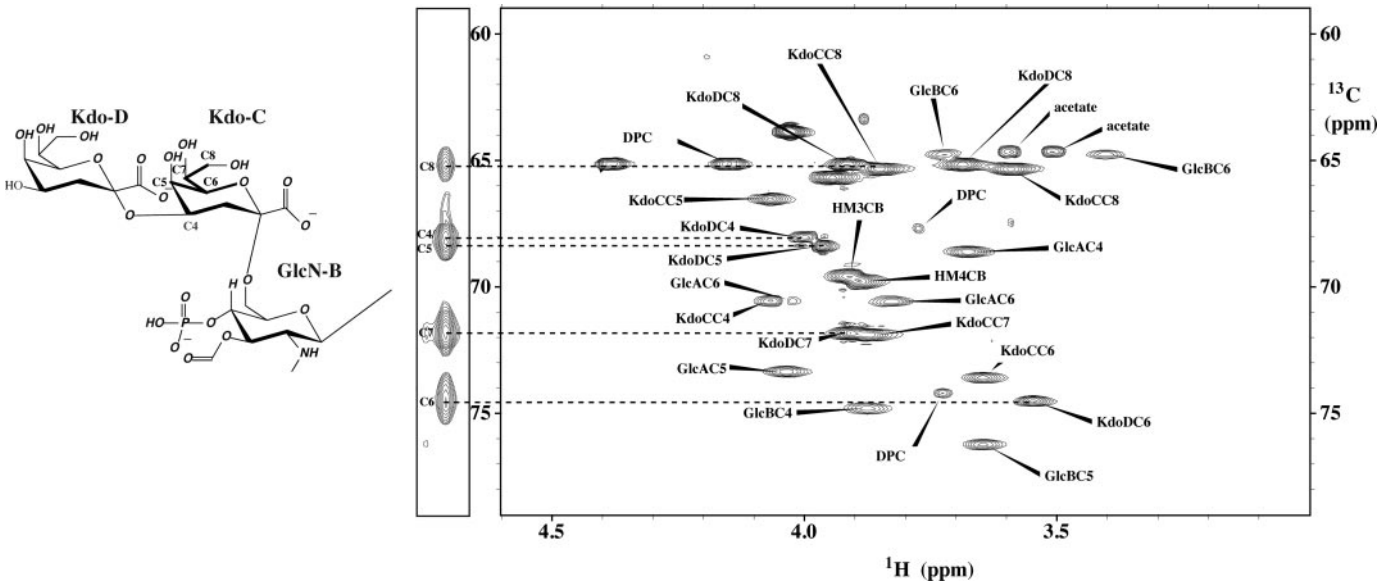

FIGURE 3. **Assignment of ^{13}C spin systems of a short stretch contained in Kdo-D from LPS using (H)CCH-TOCSY spectra.** On the right the constant-time ^{13}C,^{1}H HSQC spectrum is shown, in the middle a strip from the (H)CCH-TOCSY taken at the proton frequency of H-(C4) of Kdo-C.

TABLE 1

Carbon and proton chemical shifts of LPS from the deep-rough mutant of *E. coli*, 0.35 mM LPS in 300 mM DPC (pH 4.4), 40 mM acetate, *T* = 310 K

Sugar moieties	GlcN-A	GlcN-B	Kdo-C	Kdo-D
H1	5.346	4.681		
H2	3.928	3.861		
H3	5.143	5.072	1.900	2.104
H3			1.937	1.731
H4	3.689	3.879	4.086	4.022
H5	4.040	3.654	4.079	3.989
H6	4.018	3.409	3.647	3.550
H6	3.826	3.734		
H7			3.869	3.920
H8			3.872	3.926
H8			3.599	3.697
C1	95.56	104.41		
C2	54.05	55.61		
C3	75.43	76.03	35.33	36.50
C4	68.63	74.75	70.58	68.00
C5	73.32	76.19	66.63	68.35
C6	70.50	64.73	73.66	74.63
C7			71.89	71.77
C8			65.50	65.32

Lipid chains

	LM		MM		HM-4	HM-3
	L	HM2	M	HM1		
HA	2.306[a]	2.562	–[a]	2.643	2.312	2.383
HA		2.585	–[a]	2.670	2.366	2.433
HB	1.563[a]	5.283	–[a]	5.128	3.890	3.910
HC	1.210[a]	1.519	–[a]	1.548	1.303	1.383
HC		1.559	–[a]	1.601	1.380	1.471
HD					1.281	1.392
CA	36.51[a]	43.15	–[a]	41.10	45.38	44.18
CB	27.34[a]	72.37	–[a]	72.50	69.77	69.61
CG	31.50[a]	37.18	–[a]	36.25	38.30	40.30
CD					27.98	28.08

[a] Resonances that cannot be distinguished between L and M because of overlap.

the aqueous phase, the micelle-integrating spin label methyl 5-doxylstearate was used. The paramagnetic moiety of the spin label resides in the headgroup region (47, 48), and signal reductions in the proton-carbon correlation maps indicate proximity of the corresponding C–H moiety to the water-micelle interface. The results from the spin-label experiment are depicted in Fig. 4. Strongest attenuations of signals are observed for C and H moieties of terminal acyl-chain carbons, which are close to the GlcN sugars. Much less pronounced attenuations are observed for signals from the GlcN moieties, and the Kdo units are essentially not affected. The data demonstrate that LPS inserts into the DPC micelles such that the amide moieties of LPS are located in the headgroup region, the acyl chains are inserted into the micelle interior, and the carbohydrate units are exposed on the surface of the micelles.

We additionally probed for the topology of the polymyxin·micelle complex using the micelle-integrating spin label methyl 5-doxylstearate as described in the previous section. Notably PMX-B, -E, and -M differ only for residues in positions 6 and 7 (see legend of Fig. 1). The largest attenuations were observed for the amide moieties of the first residue, and for residues 6 and 7 in PMX-B and -E, the latter two present hydrophobic or aromatic residues (supplemental Table S13), revealing that polymyxins are attached via the N-terminal lipid chain and the apolar residues to the micelle. Note the stronger attenuations for position 7 in PMX-B and -E compared with PMX-M underscoring the importance of hydrophobic residues for partitioning into the water-membrane interface.

Interactions of LPS with Various Types of Polymyxins—As a result of exchange processes and the limited lifetime of the PMX-LPS complexes the number of intermolecular NOEs was insufficient to establish the nature of the molecular contacts. Therefore, a hybrid approach was chosen instead that included (i) chemical shift mapping data to probe for moieties involved in forming intermolecular contacts both in LPS as well as in PMX, (ii) measurement of intermolecular NOEs using isotope-filtered NOESY experiments, and (iii) restrained MD simulations of the complex of Re-LPS and PMX-B in the presence of DPC micelles, followed by selection of a subset of conformers that are compatible with the experimental data.

For chemical shift mapping purposes we initially used very simplified model compounds of LPS derived from α-(D)-glucose (Fig. 1) (49). Considering the proposed importance of

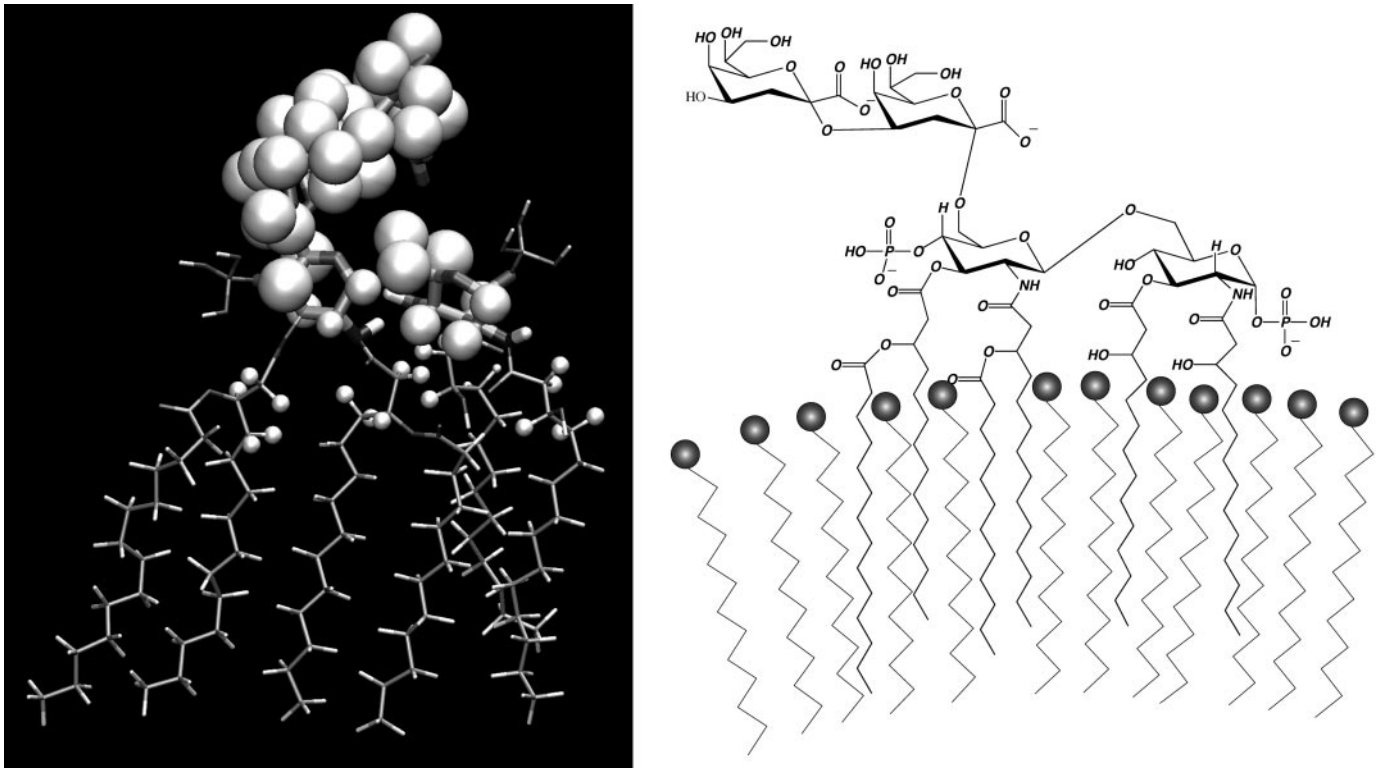

FIGURE 4. *Left*: results from the spin-label experiments displayed on the structure of LPS. The *size* of the *sphere* is proportional to the remaining signal in the proton-carbon correlation map. Because signals from ends of the fatty acid chains are not resolved in the spectra, no encoding is shown for these atoms. *Right*: sketch of LPS from the D31m4 strain when inserted into DPC micelles. The phospholipid headgroups are depicted as *gray spheres*.

phosphate moieties for binding it was not surprising that compound **3** did not display any interactions with PMX-B, but also compound **4**, which contains the presumably important phosphate group, did not cause any changes in the spectra upon addition of PMX-B, indicating that very little or no interaction exists.

Chemical shift mapping experiments using Re-LPS were performed by mixing either $^{13}C,^{15}N$-labeled LPS and unlabeled PMX-M or $^{13}C,^{15}N$-labeled PMX-M and unlabeled Re-LPS to localize the binding site within LPS or PMX-M, respectively. Unfortunately, broad lines were observed for resonances of PMX-M, indicating the presence of exchange processes and complicating assignments (see below). In contrast, resonances of Re-LPS in the complex were much narrower allowing a more detailed analysis of the shift changes such that the binding site is experimentally better defined in LPS. The chemical shift changes of LPS carbon and proton frequencies upon adding PMX-B, -E, or -M are mapped onto the structure in Fig. 5. In general, the largest changes were observed for all observable atoms of GlcN-B. Interestingly, resonances from C1 and C2 of GlcN-A were affected only very little (supplemental Fig. S3, *A–C*). In addition, resonances from Kdo-C display significantly larger changes than those of Kdo-D, with C-3 of Kdo-C being shifted by the largest extent (see supplemental Fig. S3*F*). Moreover, large changes are additionally observed for the alpha (supplemental Fig. S3*G*), beta, and gamma (supplemental Fig. S3*H*) positions of the fatty acid chains, in particular for those of HM2 (note that the second branch of MM and LM cannot be assigned due to resonance overlap). The Cα change for HM1 is less pronounced. The alpha position of HM4 was apparently more affected than of HM3. The chemical shift changes on the beta position were smaller and clear only for HM4.

A comparison of chemical shift changes of Re-LPS upon complexation with PMX-B, PMX-E, and PMX-M may serve to identify differences in their binding modes. Chemical shift changes are almost identical at positions C-4 and C-5 of GlcN-B as well as on position C-3 of Kdo-C for PMX-B and PMX-E (supplemental Fig. S3, *E* and *F*), and very similar changes occur for the alpha position of HM2. These regions are most likely in contact with the conserved parts of polymyxins. However, significant changes were observed for C-3 of GlcN-B, and moderate differences can be seen at positions of C-3, C-5, and C-6 of GlcN-A and at position C-1 of GlcN-B (supplemental Fig. S3*B*). Addition of PMX-M results in line-broadening for resonances of C-4 and C-5 of GlcN-B, as well as for C-3 of Kdo-C, and in a chemical shift change for C-6 of Kdo-C. We attribute this observation to a slightly different binding mode of PMX-M, which results in different contacts to Kdo-C.

A similar analysis for resonances of PMX-M to localize the binding site within the peptide was complicated by the above-described exchange broadening. Nevertheless, line widths in the $^{13}C,^{1}H$ HSQC spectra of PMX-M are moderate such that interactions can be detected by shift mapping methods, although some resonances remained significantly broadened and some of the shifted resonances cannot be assigned unambiguously. The results shall only be briefly summarized here: largest chemical shift changes occur for Cα resonances of residues 4, 5, 6, 8, and 9 of polymyxin-M, the members of the macrocyclic ring. Interestingly, comparably small differences were observed for resonances from the lipid chain or from Dab-1,

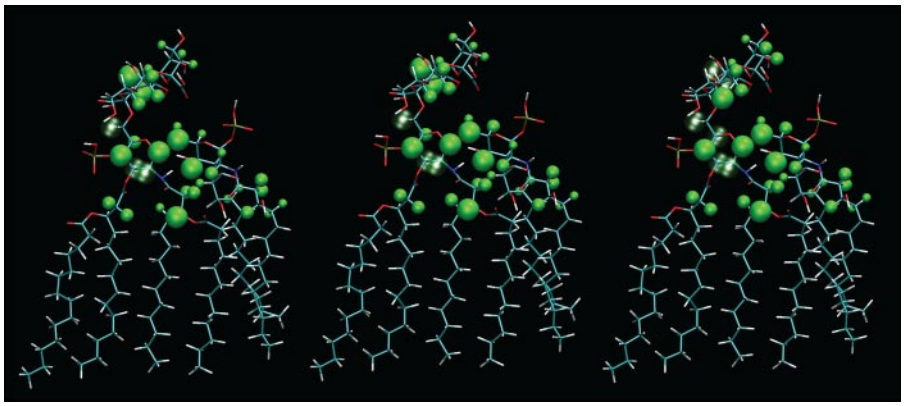

FIGURE 5. **Changes in ^{1}H and ^{13}C chemical shifts of resonances from LPS when adding PMX-B (*left*), PMX-E (*middle*), and PMX-M (*right*).** The *size* of the *spheres* is proportional to the observed differences. Deviations of peak positions were extracted from the $^{13}C,^{1}H$ HSQC spectra and computed according to $\Delta\delta$ = sqrt(($\Delta\delta$ C)^2+(10* $\Delta\delta$ ^{1}H)^2). Those atoms that are exchange-broadened beyond detection are depicted by *green transparent spheres*.

TABLE 2

Intermolecular NOEs as detected in ^{13}C-filtered NOESY experiments performed with ^{13}C-labeled LPS and unlabeled PMX-B and -E

0.5 mM LPS, 2 mM PMX, 300 mM DPC, 40 mM acetate (pH 4.4), 310 K. The strength of the NOE is classified as weak ("w"), medium ("m"), or strong ("s").

Polymyxin-B					
HM4-H(Cα)	Leu-7-Hδ1	w	HM3-H(Cγ)	Phe-6-Hε	w
HM4-H(Cβ)	Leu-7-Hδ1	s	HM3-H(Cδ)	Phe-6-Hδ	s
HM4-H(Cδ)	Leu-7-Hδ1	w	HM3-H(Cδ)	Phe-6-Hε	s
HM4-H(Cδ)	Leu-7-Hδ2	s	HM4-H(Cδ)	Phe-6-Hδ	s
HM4-H(Cγ)	Leu-7-Hδ2	s	HM4-H(Cδ)	Phe-6-Hε	w
HM4-H(Cβ)	Leu-7-Hδ2	s	HM1-H(Cβ)	Phe-6-Hδ	w
HM4-H(Cα)	Leu-7-Hδ2	s	HM4-H(Cβ)	Phe-6-Hδ	w
HM4-H(Cβ)	Leu-7-Hγ	s	HM3-H(Cγ)	Phe-6-Hδ	s
HM4-H(Cβ)	Leu-7-Hβ2	s	HM4-H(Cα)	Phe-6-Hδ	s
HM4-H(Cβ)	Leu-7-Hβ1	w	HM4-H(Cγ)	Phe-6-Hδ	s
HM3-H(Cβ)	Phe-6-Hβ2	w	HM3-H(Cα)	Phe-6-Hδ	s
HM1-H(Cβ)	Phe-6-Hβ2	w	HM3-H(Cβ)	Phe-6-Hδ	s
HM2-H(Cα)	Phe-6-Hβ1	w	HM2-H(Cα)	Phe-6-Hδ	s
HM4-H(Cα)	DABA8-Hγ	s	HM2-H(Cβ)	Phe-6-Hε	w
HM4-H(Cβ)	DABA8-Hγ	w	HM4-H(Cα)	DABA8-HN	w
HM4-H(Cγ)	Phe-6-Hε	w			
Polymyxin-E					
HM4-H(Cα)	Leu-6-Hδ1	m	HM2-H(Cα)	Leu-6-Hδ1	s
HM4-H(Cα)	Leu-7-Hβ	m	HM2-H(Cα)	Leu-6-HN	m
HM4-H(Cβ)	Leu-6-Hγ	m	HM2-H(Cα)	Leu-6-Hγ	m
HM4-H(Cβ)	Leu-7-Hβ	m	HM2-H(Cβ)	Leu-6-Hγ	m
HM4-H(Cβ)	Leu-7-Hδ1	m	HM1-H(Cγ)	Dab-4-HN	w
HM4-H(Cβ)	Leu-7-Hγ	w	HM1-H(Cγ)	Leu-6-HN	m
HM4-H(Cβ)	Leu-7-HN	m	HM3-H(Cα)	Leu-6-Hδ1	m
HM4-H(Cδ)	Leu-7-Hβ	w	HM3-H(Cβ)	Leu-6-Hδ1	m
HM4-H(Cγ)	Leu-6-Hδ1	s	HM3-H(Cγ)	Leu-6-Hδ1	m

Thr-2, or Dab-3. The fact that only residues from the macrocycle experience large changes indicates that the heptapeptide ring of PMX binds to LPS. Our data additionally support the view that the interaction is primarily electrostatic (50): $^{15}N,^{1}H$ HSQC spectra of PMX-M initially used to screen conditions displayed multiple peaks and very broad lines. However, in the presence of 20 mM $MgCl_2$ electrostatic interactions were largely screened and a good quality $^{15}N,^{1}H$ HSQC spectrum of PMX-M was obtained with peak positions close to those in the absence of LPS.

Interactions between Re-LPS and polymyxin were additionally directly detected by measuring intermolecular NOEs between unlabeled PMX-E or -B and $^{13}C,^{15}N$-labeled LPS using isotope-filtered NOESY experiments (see Table 2 and supplemental Fig. S7). Interestingly, in the case of PMX-B, NOEs between side-chain protons of Phe-6 or Leu-7 and the lipid chains of LPS are detected (see supplemental Fig. S7). A number of NOEs between protons of the π-system of Phe-6 and the lipid chains are observed, in particular to Cγ of HM2 and Cα of HM3. The fact that PMX-B or PMX-E form many contacts with LPS that involve side chains of residues 6 and 7 indicates that the hydrophobic nature of these side chains may be important for orienting polymyxin in the complex with LPS. Unfortunately, larger line widths in the LPS·PMX-M complex precluded the measurement of isotope-filtered NOESY spectra in that case.

Restrained Molecular Dynamics Calculations—To obtain a first picture of the complex formed between LPS and PMX-B we have performed a MD calculation in which LPS was docked to PMX-B using NOE-derived upper distance limits (Fig. 6) in the presence of a DPC micelle. In the complex backbone amide moieties of the peptide macrocycle form contacts with the phosphate group of GlcN-B. Residues from one hydrophobic site, D-Phe-6 and Leu-7, are in proximity to the fatty acid chains of LPS. Leu-7 makes additional contacts with the GlcN-B moiety. The amino group of Dab-8 is involved in electrostatic contacts with the phosphate group at GlcN-A. Amino groups of Dab-9 and -3 are possibly forming electrostatic interactions with the carboxyl group of Kdo-C. The backbone of residues Dab-1 to Dab-3 is located in the acyl region of the branched fatty acids originating from GlcN-B. To summarize, most contacts in this model structure are made with GlcN-B and the adjacent atoms of GlcN-A, as well as with parts of Kdo-C. The model structure is supported by the chemical shift mapping data and the intermolecular NOEs. In addition, interacting moieties of LPS that make contacts common with all polymyxin variants are in contact with conserved parts of these peptides (residues 1–4 and 8–10), whereas those sites, that differ in their interaction with the different peptides form contacts with non-conserved residues.

DISCUSSION

In this work we have used polymyxins of different types and a combination of NMR spectroscopy and restrained molecular dynamics to study their interactions with LPS from the deep rough mutant *E. coli* strain. To our knowledge this work for the first time presents experimental data on the interacting moieties in a membrane mimetic environment.

The conformation of LPS-bound PMX-B and -E was elucidated previously using transfer-NOE techniques by Pristovsek (11). Therein, the LPS-bound peptides assume envelope-like bent cycles that separate the two hydrophobic residues 6 and 7 from the charged Dab residues 4, 5, 8, and 9. The conformation from the transfer NOE-derived structure was then docked onto a lipid A model. In the resulting complex the lipid chain of PMX forms transient contacts with acyl chains A and B from lipid A. Moreover, the two phosphate groups are in close contact with

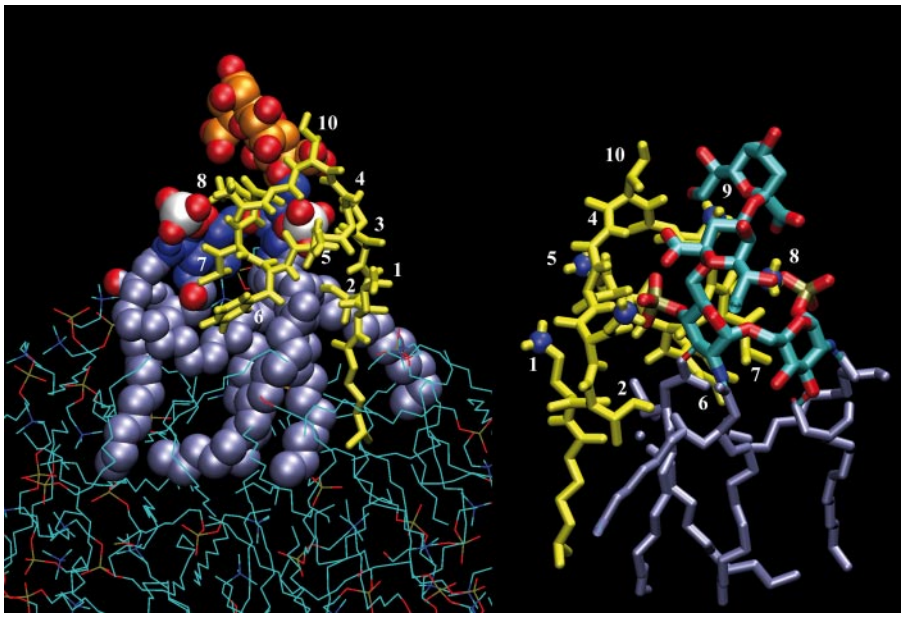

FIGURE 6. *Left*: structure of the PMX-B·LPS complex as derived from the MD calculation. The covalent structure of PMX-B is depicted in *yellow*. Heavy atoms of LPS are drawn as van der Waals *spheres*, with lipid chains colored in *ice blue*, GlcN carbons in *dark blue*, Kdo carbons in *orange*, and phosphorous atoms in *white*. DPC molecules are indicated by *thin lines*. Residue numbers of PMX-B are placed close to the corresponding side chains. *Right*: representation showing only bonds of LPS and PMX-B. PMX-B is again drawn in *yellow*, with amino nitrogens of DAB residues in *blue*, while LPS bonds are drawn in *ice blue* (lipids) or *green* (sugar parts).

the γ-NH_2 groups of Dab residues 1/5 and 8/9. Their data highlight the importance of electrostatic interactions between phosphate groups and amino groups of polymyxin as well as hydrophobic interactions of the lipid chains with Phe or Leu residues. Martin *et al.* (19) have studied the structure of LPS-bound PMX-M, which displayed a chair-like conformation, in which the side chain of Dab-4 or -8 and Leu-6 or Thr-7 point into the opposite directions in a fashion similar to that proposed for PMX-B and -E (19). Pristovsek determined the structure of a LPS-bound synthetic fragment of the LALF protein (10) revealing a hairpin-type fold, again characterized by spatial separation of hydrophobic and cationic residues. In another study Bhunia *et al.* (7) investigated binding of melittin to LPS micelles. Cationic residues have also been postulated to critically contribute to binding of LPS to proteins such as MD-2 (51) or FhuA (16, 52).

Herein we set out to determine interactions between LPS and polymyxins in more detail. Considering that interacting chemical moieties have not been experimentally identified with confidence so far we reasoned that these studies should use chemically defined environments in a setup that mimics natural conditions. To achieve chemical homogeneity we developed a novel chromatographic separation procedure that does not require methylation of phosphates. To facilitate isotope labeling biosynthetic LPS was used. LPS from the deep rough mutant of *E. coli* presents a simple system containing all chemical moieties believed to be important for the interaction, and in the absence of phospholipids has been assigned previously using homonuclear two-dimensional NMR techniques (17, 18). LPS in Gram-negative bacteria is embedded in a phospholipid bilayer, and therefore the system was studied in DPC micelles. Our data reveal that LPS inserts into the micelle via integration of the acyl chains into the micelle interior, and that the GlcN and Kdo portions are fully exposed in the aqueous compartment. Using ^{13}C isotope labeling we have been able to fully assign LPS while integrated into DPC micelles. In the latter environment spectra with reasonable line widths and resolution for LPS can be recorded. Spectroscopic features of peptide resonances of PMX were less favorable but, in combination with restrained MD calculations, allowed studying interactions in sufficient detail.

The chemical shift-mapping data (Fig. 5), the intermolecular NOEs (Table 2), and the model derived from molecular dynamics restrained by these experimental data (Fig. 6 and supplemental Fig. S9) now support the structure of the PMX-B·LPS complex as proposed by Pristovsek *et al.* (11) in most but not all of its details. In their complex the macrocycle of PMX-B covers the GlcN disaccharide unit, and hydrophobic side chains of polymyxin form contacts with the lipid chains from LPS. A similar complex topology was proposed for the interaction of LPS with PMX-M (19). Such an arrangement is facilitated by the amphiphilic nature of PMX, in which hydrophobic and hydrophilic side chains point into opposite directions. A similar separation of hydrophobic and hydrophilic moieties in LPS helps to orient the two molecules with respect to each other through hydrophobicity matching. Interestingly, in a phospholipid environment such effects are even amplified, because similar requirements influence binding of polymyxin to phospholipids surface or to LPS. Accordingly, Leu or Phe residues, for which favorable energies for partitioning into the membrane interior or the water-membrane interfacial region have been measured (53), form contacts with the α, β, and γ acyl chain carbons of LPS, as evident from both large changes in the chemical shift mapping experiments as well as from the corresponding intermolecular NOEs. In PMX-M position 7 is occupied by Thr, a much more polar residue. According to the data from this work, PMX-M may be slightly differently oriented, possibly forming somewhat stronger contacts with the Kdo units thereby compensating for loss of interaction energy with the acyl chains. In the PMX-M·LPS complex electrostatic or polar interactions involving the Dab residues of polymyxin and the carbohydrate moieties of GlcN-B or Kdo-C and to a smaller extent, Kdo-D dominate, whereas in the case of PMX-B or -E additional hydrophobic interactions from side chains of Leu-7 are likely to contribute to binding. Although our work confirmed the contacts made with moieties of the GlcN units proposed in the model complex from Pristovsek (11), it is different in that it emphasizes the importance of contacts to Kdo units, in particular to Kdo-C.

Different models have been proposed for the mechanism of action of polymyxin. Shai *et al.* have proposed that binding of polymyxin to the core part of LPS, lipid A, results in disturbance of the LPS-phospholipid bilayer destroying the integrity of the outer membrane, and possibly leading to pore formation (9, 13). The orientation of LPS in the phospholipid micelles as measured using spin labels has demonstrated that the carbonyl group region of the LPS lipid chains is located in the headgroup region. Binding of polymyxin to LPS therefore places the amphiphilic peptide in a similar position compared with binding to pure phospholipid micelles. Accordingly, similar mechanisms for membrane permeabilization are plausible.

Acknowledgments—We are very grateful to John C. Vederas for supplying us with cells producing polymyxin M and John Robinson and Reto Walser for helpful discussions.

Note Added in Proof—Recently Grzesiek's group has determined the structure of a highly similar LPS in dihexanoylphosphatidylcholine micelles (Wang, W., Sass, H. J., Zäbringer, U., and Grzesiek, S. (2008) Angew. Chem. Int. Ed. Engl. **47,** 9870–9874).

REFERENCES

1. Gennis, R. B. (1989) *Biomembranes: Molecular Structure and Function*, Springer, New York
2. Yeagle, P. L. (1993) *The Membranes of Cells*, Academic Press, San Diego, CA
3. Raetz, C. R., Garrett, T. A., Reynolds, C. M., Shaw, W. A., Moore, J. D., Smith, D. C., Ribeiro, A. A., Murphy, R. C., Ulevitch, R. J., Fearns, C., Reichart, D., Glass, C. K., Benner, C., Subramaniam, S., Harkewicz, R., Bowers-Gentry, R. C., Buczynski, M. W., Cooper, J. A., Deems, R. A., and Dennis, E. A. (2006) *J. Lipid Res.* **47,** 1097–1111
4. David, S. A. (2001) *J. Mol. Recognit.* **14,** 370–387
5. Andra, J., Lohner, K., Blondelle, S. E., Jerala, R., Moriyon, I., Koch, M. H., Garidel, P., and Brandenburg, K. (2005) *Biochem. J.* **385,** 135–143
6. Bhattacharjya, S., Domadia, P. N., Bhunia, A., Malladi, S., and David, S. A. (2007) *Biochemistry* **46,** 5864–5874
7. Bhunia, A., Domadia, P. N., and Bhattacharjya, S. (2007) *Biochim. Biophys. Acta* **1768,** 3282–3291
8. Ding, L., Yang, L., Weiss, T. M., Waring, A. J., Lehrer, R. I., and Huang, H. W. (2003) *Biochemistry* **42,** 12251–12259
9. Papo, N., and Shai, Y. (2005) *J. Biol. Chem.* **280,** 10378–10387
10. Pristovsek, P., Feher, K., Szilagyi, L., and Kidric, J. (2005) *J. Med. Chem.* **48,** 1666–1670
11. Pristovsek, P., and Kidric, J. (1999) *J. Med. Chem.* **42,** 4604–4613
12. Rana, F. R., and Blazyk, J. (1991) *FEBS Lett.* **293,** 11–15
13. Rosenfeld, Y., Papo, N., and Shai, Y. (2006) *J. Biol. Chem.* **281,** 1636–1643
14. Rosenfeld, Y., and Shai, Y. (2006) *Biochim. Biophys. Acta* **1758,** 1513–1522
15. Wang, H., Head, J., Kosma, P., Brade, H., Muller-Loennies, S., Sheikh, S., McDonald, B., Smith, K., Cafarella, T., Seaton, B., and Crouch, E. (2008) *Biochemistry* **47,** 710–720
16. Ferguson, A. D., Hofmann, E., Coulton, J. W., Diederichs, K., and Welte, W. (1998) *Science* **282,** 2215–2220
17. Qureshi, N., Takayama, K., Mascagni, P., Honovich, J., Wong, R., and Cotter, R. J. (1988) *J. Biol. Chem.* **263,** 11971–11976
18. Agrawal, A. B., Qureshi, N., and Takayama, K. (1998) *Magn. Reson. Chem.* **36,** 1–7
19. Martin, N. I., Hu, H. J., Moake, M. M., Churey, J. J., Whittal, R., Worobo, R. W., and Vederas, J. C. (2003) *J. Biol. Chem.* **278,** 13124–13132
20. Live, D. H., Davis, D. G., Agosta, W. C., and Cowburn, D. (1984) *J. Am. Chem. Soc.* **106,** 6104–6105
21. Keller, R. (2004) *The Computer Aided Resonance Assignment*, Cantina Verlag, Goldau
22. Goddard, T. D., and Kneller, D. G. (2006) *Sparky 3*, Version 3.113, University of California, San Francisco, CA
23. Keeler, J., Clowes, R. T., Davis, A. L., and Laue, E. D. (1994) *Methods Enzymol.* **239,** 145–207
24. Palmer, A. G., Cavanagh, J., Wright, P. E., and Rance, M. (1991) *J. Magn. Reson.* **93,** 151–170
25. Kay, L. E., Keifer, P., and Saarien, T. (1992) *J. Am. Chem. Soc.* **114,** 10663–10665
26. Yamazaki, T., Lee, W., Arrowsmith, C. H., Muhandiram, D. R., and Kay, L. E. (1994) *J. Am. Chem. Soc.* **116,** 11655–11666
27. Wittekind, M., and Mueller, L. (1993) *J. Magn. Reson. Ser. B* **101,** 201–205
28. Bax, A., Clore, G. M., Driscoll, P. C., Gronenborn, A. M., Ikura, M., and Kay, L. E. (1990) *J. Magn. Reson.* **87,** 620–627
29. Olejniczak, E. T., Xu, R. X., and Fesik, S. W. (1992) *J. Biomol. NMR* **2,** 655–659
30. Hess, B., Kutzner, C., van, d. S., David and Lindahl, E. (2008) *J. Chem. Theory Comput.* **4,** 435–447
31. Hassinen, T., and Perakyla, M. (2001) *J. Comput. Chem.* **22,** 1229–1242
32. Schüttelkopf, A. W., and van Aalten, D. M. F. (2004) *Acta Crystallogr. D Biol. Crystallogr.* **60,** 1355–1363
33. Oostenbrink, C., Villa, A., Mark, A. E., and van Gunsteren, W. F. (2004) *J. Comp. Chem.* **25,** 1656–1676
34. Gasteiger, J., and Marsili, M. (1980) *Tetrahedron* **36,** 3219–3228
35. No, K. T., Grant, J. A., and Scheraga, H. A. (1990) *J. Phys. Chem.* **94,** 4732–4739
36. Galanos, C., Luderitz, O., and Westphal, O. (1969) *Eur. J. Biochem.* **9,** 245–249
37. Shuker, S. B., Hajduk, P. J., Meadows, R. P., and Fesik, S. W. (1996) *Science* **274,** 1531–1534
38. Clore, G. M., and Gronenborn, A. M. (1982) *J. Magn. Reson.* **48,** 402–417
39. Clore, G. M., and Gronenborn, A. M. (1983) *J. Magn. Reson.* **53,** 423–442
40. Otting, G., and Wüthrich, K. (1990) *Q. Rev. Biophys.* **23,** 39–96
41. Marchioro, C., Davalli, S., Provera, S., Heller, M., Ross, A., and Senn, H. (2003) in *BioNMR in Drug Research* (Zerbe, O., ed) pp. 321–340, Wiley-VCH, Weinheim, Germany
42. Blommers, M. J. J., and Rüdisser, S. (2003) in *BioNMR in Drug Research* (Zerbe, O., ed) pp. 355–372, Wiley-VCH, Weinheim, Germany
43. Gemmecker, G. (2003) in *BioNMR in Drug Research* (Zerbe, O., ed.) pp. 373–390, Wiley-VCH, Weinheim, Germany
44. Vuister, G. W., and Bax, A. (1992) *J. Magn. Reson.* **98,** 428–435
45. Grzesiek, S., and Bax, A. (1992) *J. Magn. Reson.* **96,** 432–440
46. Kay, L. E., Ikura, M., Tschudin, R., and Bax, A. (1990) *J. Magn. Reson.* **89,** 496
47. Papavoine, C. H., Konings, R. N., Hilbers, C. W., and van de Veen, F. J. (1994) *Biochemistry* **33,** 12990–12997
48. Jarvet, J., Zdunek, J., Damberg, P., and Gräslund, A. (1997) *Biochemistry* **36,** 8153–8163
49. Gobbo, M., Biondi, L., Filira, F., and Rocchi, R. (2006) *J. Pept. Sci.* **12,** 132–139
50. Koch, P. J., Frank, J., Schuler, J., Kahle, C., and Bradaczek, H. (1999) *J. Colloid Interf. Sci.* **213,** 557–564
51. Gruber, A., Mancek, M., Wagner, H., Kirschning, C. J., and Jerala, R. (2004) *J. Biol. Chem.* **279,** 28475–28482
52. Ferguson, A. D., Welte, W., Hofmann, E., Lindner, B., Holst, O., Coulton, J. W., and Diederichs, K. (2000) *Structure* **8,** 585–592
53. Wimley, W. C., and White, S. H. (1996) *Nat. Struct. Biol.* **3,** 842–848